PAPER • OPEN ACCESS

Laser-Optical Shear-Flow Analysis across the Annular Gap of a Simplified Displacement Compressor Model

To cite this article: Robin Leister *et al* 2022 *IOP Conf. Ser.: Mater. Sci. Eng.* **1267** 012003

View the article online for updates and enhancements.

Laser-Optical Shear-Flow Analysis across the Annular Gap of a Simplified Displacement Compressor Model

Robin Leister[1], Andreas Brümmer[2], Jochen Kriegseis[1*]

[1] Institute of Fluids Mechanics (ISTM), Karlsruhe Institute of Technology (KIT), Kaiserstr. 10, 76131 Karlsruhe, Germany

[2] Chair of Fluidics (FT), TU Dortmund University (TUD), Leonhard-Euler-Str. 5, 44227 Dortmund, Germany

E-mail: `kriegseis@kit.edu`

Abstract. The present experimental feasibility study testifies the two flow measurement techniques Defocusing Particle Tracking Velocimetry (DPTV) and Interferometric Particle Imaging (IPI) for their applicability to measure the two-phase flow of thin (sub-millimeter) annular rotor-stator gaps such as occur across for the leakage flow e.g. in the housing gap of oil-injected rotary positive displacement compressors (RPDC). To provide unrestriced optical access to the annular gap and in turn eliminate secondary effects, a simplified displacement compressor model has been developed and fabricated from perspex. The proof-of-concept results of both experimental campaigns (DPTV & IPI) are discussed and avenues for future efforts towards a straight-forward and accurate applicability of either method are elaborated.

1. Introduction

The efficiency of oil-injected rotary positive displacement compressors (RPDC) is dominated by surge- and gap-flow phenomena between adjacent chambers. To improve both prediction and optimization strategies towards further RPDC advances, an in-depth knowledge of the involved flow patterns across e.g. the annular rotor-stator gap (rotor-housing gap) is of utmost importance. However, experimental data for RPDCs rely on integral measures as basis for modeling efforts and are at most supported by qualitative visualizations of the respective flow regimes. Valuable reports on such combined qualitative visualizations and integral torque measures have been provided e.g. by Xin *et al.* [1] and Vasuthevan & Brümmer [2], which as yet generally remain to be complemented with spatio-temporally resolved void-fraction and velocity information.

Typical flow-measurement techniques encounter limitations when applied to wide aspect-ratio gap flows, where a single microscopic characteristic length scale, i.e. the annular gap, is accompanied by macroscopic characteristic length scales along the lateral surface. The curved boundaries of the annular rotor-stator gap and limited optical access further render the given flow scenario particularly challenging for a quantitative analysis of the involved multiphase-flow phenomena as occur across such narrow gaps. Recently, a similarly challenging flow scenario inside the 540 µm wide rotor-stator gap of an open wet clutch has been successfully analyzed experimentally by Leister *et al.* [3] with phase-resolved defocusing particle tracking

velocimetry (DPTV) [4, 5], where the recorded volumetric three-component velocity information uncovered vortical structures and related implications on the adverse drag-torque generation of the considered clutch.

As for RPDCs, additional complexity comes into play due to the two-phase character of bubble growth, bubble-bubble and bubble-wall interactions, all of which requires additional complementary measurement techniques to further account for the identification of the gas phase (onset) in the gap. For small gas particles, where shadowgraphy-based sizing of particles is limited (if possible at all), interferometric particle imaging (IPI) has proven applicability for image-based particle-size analysis [6], which is well established for spray characterization [7], but was also applied for bubble-sizing studies [8, 9].

The present study addresses the aforementioned lack of quantitative void-fraction and velocity data in the annular gap of RPDCs by means of a proof-of-concept measurement campaign. First, the DPTV approach – as developed by Leister *et al.* [3] for thin rotor-stator configurations – is adapted and tested for the investigation of curved, i.e. annular, gap flows. In a second step, this DPTV-setup is chosen to furthermore provide a first indicator of the general applicability of IPI measurements for bubble (-growth) investigations in thin annular rotor-stator gaps of RPDCs.

2. Experimental Procedure
First the test facility and experimental setup are introduced in Section 2.1, before the two considered measurement techniques, i.e. Defocusing Particle Tracking Velocimetry (DPTV) and Interferometric Particle Imaging (IPI) are briefly recapped in Section 2.2 and 2.3, respectively.

2.1. Experimental Setup
In order to provide a straight-forward applicable test scenario for the present study, a simplified RPDC model tabletop test facility has been built for the experiments, which is comprised of a rotating perspex cylinder (diameter $39\,\text{mm}$), a cylindrical perspex container (inner diameter $60\,\text{mm}$, wall thickness $8\,\text{mm}$) and a *Bosch PBD 40* tabletop drill press to operate the rotor at an adjustable angular velocity of $\Omega = 21\,\text{s}^{-1}$. To avoid any tumbling issues during operation, the rotor was first assembled in the drill chuck, and then in-situ evened with metal-lathe tool bits and subsequently polished while spinning. The container was eccentrically adjusted on the base plate of the drill to provide a $h = 200\,\mu\text{m}$ gap height at the smallest cross-section for the measurements. The experimental setup for the conducted DPTV and IPI measurements is shown in Figure 1, which further indicates the angular arrangement of the optical components.

A *PCO Pixelfly* camera (14 bit, maximum resolution 1392×1040 pixels) equipped with a *Nikon Nikkor* lens captured a 8.2×6.1 mm^2 field of view (FOV) of the smallest cross-section of the annular gap, where the optical axis was aligned with the radial coordinate of both rotor and stator cylinders. The FOV was illuminated with the raw beam of a *Quantel EverGreen* Nd:YAG ($\lambda = 532\,\text{nm}$, $200\,\text{mJ}$) dual-cavity laser at an angle range of $\theta = 92° - 100°$ to the camera axis to ensure reasonable fringe intensities for the IPI results [8]. The (single-phase) DPTV experiments were conducted with a white mineral oil (density $\varrho_o = 850\,\text{kg/m}^3$, dyn. viscosity $\mu_o = 0.0136\,\text{kg/ms}$ at $40°C$, CAS No: 8042-47-5), which was seeded with fluorescent particles of mean diameter $d_\text{p} = 9.84\,\mu\text{m}$ (density $\varrho_p = 1510\,\text{kg/m}^3$, particle response time $\tau_p = 0.6\,\mu\text{s}$, emission wave length $\lambda_e = 584\,\text{nm}$) to avoid reflections. To promote the formation of bubbles in the gap during the IPI tests, the oil was replaced with H_2CO_3-supplied water (density $\varrho_w = 993\,\text{kg/m}^3$, dyn. viscosity $\mu_w = 6.5 \times 10^{-4}\,\text{kg/ms}$ at $40°C$, refractive index $m = 1.33$) between the two experimental campaigns. The relevant experimental parameters are summarized in Table 1.
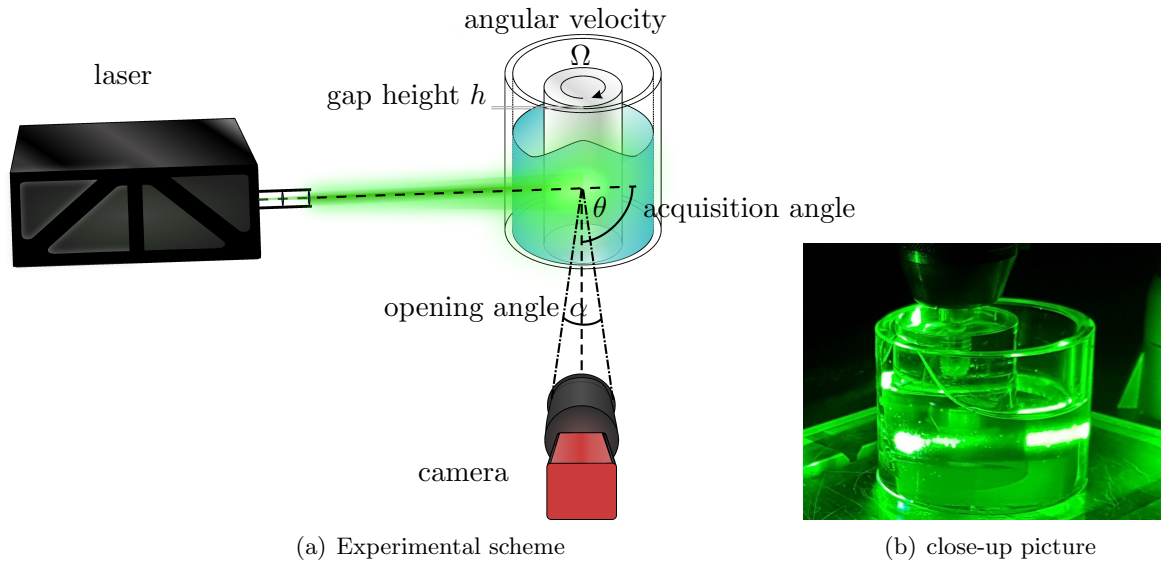
(a) Experimental scheme

(b) close-up picture

Figure 1. Experimental setup for DPTV and IPI measurements; (a) Sketch of test setup, utilized equipment and relevant parameters; (b) picture during DPTV experimentation.

Table 1. List of experimental parameters and respectively chosen liquids for the DPTV and IPI measurements.

Exp.	Quantity	Value
DPTV & IPI	angular rotor velocity	200 rpm $\widehat{=}$ 21 s^{-1}
	inner gap radius R_1 (rotor)	19.5 mm
	outer gap radius R_2 (stator)	30 mm
	laser-pulse delay Δt	300 µs
	image magnification M	1.1
	Field of View	8.2×6.1 mm^2
	expected displacement ΔX at rotor	20.7 px
DPTV	particle image diameter at $z = 0$ (stator)	43.7 px
	particle image diameter at $z = h$ (rotor)	56.2 px
	radial gap height h	200 µm
	Nikon Nikkor lens	105 mm f/2.8
	$f_\#$-number	2.8
	aperture diameter D_a	37.5 mm
	white mineral oil: dyn. viscosity	$\mu_o = 0.0136$ kg/ms (at 40°C)
	density	$\varrho_o = 850$ kg/m^3
	CAS No.	8042-47-5
IPI	fringe-pattern diameter	≈ 42 px
	radial gap height h	400 µm
	Nikon Nikkor lens	200 mm f/4
	H$_2$CO$_3$-supplied water: dyn. viscosity	$\mu_w = 6.5 \times 10^{-4}$ kg/ms (at 40°C)
	density	$\varrho_w = 993$ kg/m^3
	refractive index	$m = 1.33$

2.2. DPTV Summary

DPTV is a single-camera measurement technique for volumetric velocity measurements, which uses purposely defocused particle images to gain additional depth-localization information out of one image pair acquisition [10]. First introduced by Willert & Gharib [11] in the approach gained popularity as macroscopic, but even more as microscopic measurement technique.

A theoretical mathematical description of the diameter estimation d_i of a particle image under absence of optical aberrations is a sum of three terms, that contribute significantly to the diameter change. This relationship has been summarized by Olsen & Adrian [12] and can be written as

$$d_i^2 = \underbrace{M^2\,d_p^{\,2}}_{\text{geometric image}} + \underbrace{5.95\,(M+1)^2\,\lambda^2 f_\#^2}_{\text{diffraction}} + \underbrace{\frac{M^2 z^{*2} D_a^{\,2}}{(s_0 + z^*)^2}}_{\text{defocusing}}, \tag{1}$$

where M appears as magnification, d_p as physical particle diameter, λ as wave length of the emitted light and $f_\#$ presents the focal number of the lens. The third term is modeling the out-of-focus behavior and describes the diameter change of the particle on the image plane as function of the distance z^* between the particle and the focal plane, the distance s_0 between the lens and the focal plane, and the physical diameter of the used aperture D_a.

For practical defocusing measurements this equation can be simplified further, since $s_0 \gg z^*$ applies for any optical set-up of typical imaging applications, which reduces Equation (1) to the approximation

$$d_i(z^*) \propto \left(\text{const.} + z^{*2}\right)^{1/2}. \tag{2}$$

This hyperbola can be approximated as linear interdependence when considering out-of-focus elements that have a sufficient distance to the focal plane. Equation (2) can thus be simplified to

$$d_i(z^*) \propto z^*. \tag{3}$$

Consequently, a linear relationship between the imaged diameter and the z-axis position holds true. The actual proportionality coefficient between these two physical values can be estimated with the theoretical equation (1), but this formula is derived under the absence of optical aberrations. Accordingly, the direct use would lead to relatively high deviations, since a large array of imaging errors are present for every real camera set-up (like field curvature or spherical aberrations). To overcome this problem and link the diameter to a value in physical space the in-situ calibration approach of Fuchs et al. [4] is used, where the diameters are linked locally to the expected boundary conditions of the flow under consideration. Note that this approach in combination with the Hough-Transform [13] only compensates errors due to set-up misalignment or lens-inherent imperfections. Systematically induced astigmatic aberrations by e.g. the curvature of the test rig, however, requires additional more advanced correction methods, as outlined below.

2.3. IPI Summary

The idea and working principle of IPI goes back to the initial reports by e.g. König et al. [14] and Ragucci et al. [15], and takes advantage of the interference of two scattering orders if small particles, i.e. droplets in gas or bubbles in liquids, are illuminated with a single beam of coherent polarized light [6].

If imaged in the focal plane at a carefully chosen acquisition angle θ between illumination-beam and observation directions (cp. Figure 1(a)), the reflection glare point and the first refraction glare point (after crossing the particle) of the observed particle result in the focused image of two separated glare points of similar light intensities. Since the spatial distance of these two points is in the range of the particle diameter, the immediate quantification of the distance
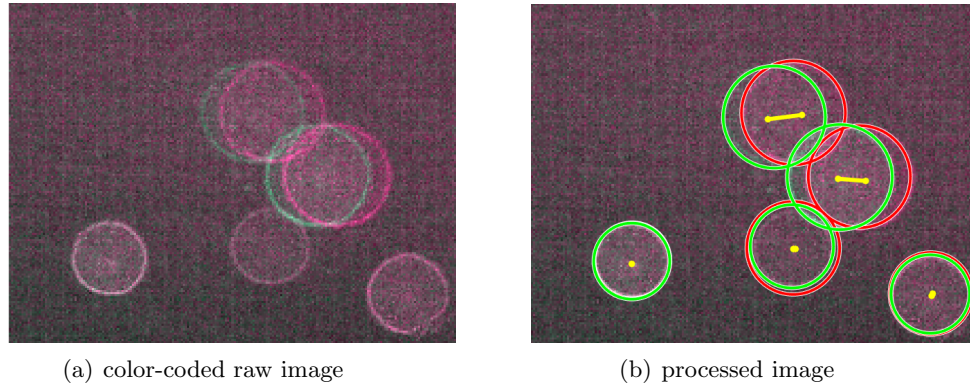
(a) color-coded raw image

(b) processed image

Figure 2. DPTV results; (a) recorded elliptical particle image, (b) processed image with detected particles and calculated displacements ΔX (yellow).

suffers heavily from the limited spatial resolution of the imaging equipment at hand and the competing goal to observe sufficiently large wide aspect-ratio FOV at accordingly lower spatial resolution.

To overcome these conflicting requirements, the particles – and thus the corresponding pairs of two glare points – are recorded with sufficient displacement from the focal plane of the imaging device. If the distance to the focal plane is large in comparison to the glare-point spacing, both glare points collapse to a single quasi-circular defocused particle, which is further comprised of an interference fringe pattern. As already outlined in Section 2.2, the diameter of the resulting fringe patterns scales with the distance of the focal plane. The number of fringes N inside each defocused particle image, moreover, scales with the diameter of the respective particle, which can be determined for bubbles diameters d_b according to

$$d_b = \frac{2\lambda N}{\alpha} \left[m \cos\left(\frac{\theta}{2}\right) - \frac{m \sin\left(\frac{\theta}{2}\right)}{\sqrt{m^2 - 2m \cos\left(\frac{\theta}{2}\right) + 1}} \right]^{-1}. \tag{4}$$

In addition to the above-introduced quantities, α appears in Equation (4), which corresponds to the collecting angle of the chosen camera lens as indicated in Figure 1(a). It is furthermore important to note that Equation (4) is only valid for the presently considered bubbles in liquid, since internal refraction inside droplets and bubbles leads to different beam paths as elaborated thoroughly by Kawaguchi *et al.* [9].

3. Results
The circles of either experimental approach are detected by means of the Hough-Transform [13], which provides information on both diameter and center of the recorded circles. This procedure has been shown to have sub-pixel accuracy, such that no issues due to pixel locking occur due to the chosen processing strategy (cp. Leister & Kriegseis [16]).

Figure 2(a) shows a random double-frame image of the DPTV measurements, where both raw images are superimposed and color coded to indicate the particle displacement between the first (red) and second (green) frame (flow from right to left, cp. Figure 1(a)). The resulting circle estimations from the Hough-Transform are added to the double frame in Figure 2(b). Furthermore, the center locations of each circle are indicated with a yellow dot. Also, the
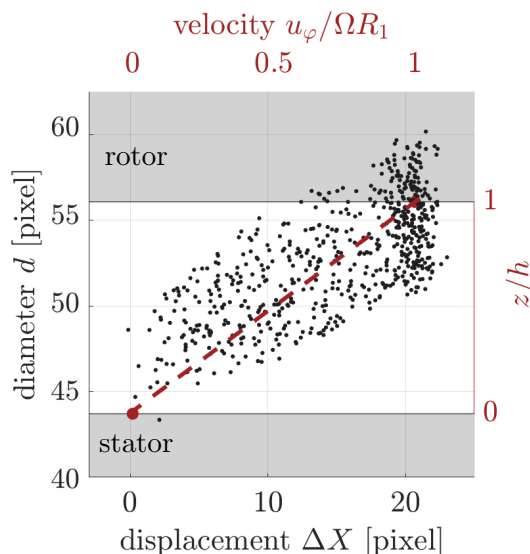
Figure 3. Resulting displacement distribution of the DPTV measurements and corresponding velocity profile across the gap; • raw data points, — — resulting velocity profile $u_\varphi(r)$, ▨ transparent walls.

tracks of the particle displacements are plotted as yellow lines connecting the center locations. The images of Figure 2 already outline that the depth codification of the particle images in combination with the detected particle displacements reveal larger particle velocities in proximity of the rotor (large circles), whereas the near-constant locations of the smaller circle-pairs indicate the vicinity to the outer stator wall.

The results from the combined depth-codification and velocity estimation are shown in Figure 3. The scatter margin ($\approx 4\,\mathrm{px}$) of the data points indicates the limited accuracy of the circle-detection based evaluation approach. Recall, that the curved stator wall introduces astigmatism to the optical system, which in turn leads to ellipse-shaped defocused particle images. Note that the high number of registered events for $u_\varphi/\Omega R_1 = 1$ furthermore stem from the number of particle, which were sticking to the rotor wall during experimentation. The vertically stretched shape of denser particle cloud around $u_\varphi/\Omega R_1 = 1$ further confirms the depth-codification estimation uncertainty to be the main contributor to the overall measurement uncertainty, since the small horizontal margin gives rise to an accurate velocity estimation of the sticking particles. The resulting fitted velocity profile, however, resembles a laminar (Poiseuille-) Couette flow, which is in accordance with Reynolds-equation considerations of the given flow scenario [17]. The pressure-driven Poiseuille flow component is to be classified as low in this case.

The feasibility tests of the IPI method for an applicability of bubble sizing and eventually tracking in thin curved annular rotor-stator gaps has been done with the identical DPTV setup, where the tracer-laden oil has been replaced by H_2CO_3-supplied water to promote the generation of bubbles in the shear flow. Some example IPI recordings are shown in Figure 4. Similar to the DPTV processing, the circular fringe pattern can be identified via the Hough-Transform [13]. Once identified, the fringe number can be quantified by means of gray-value evaluation across the diameter of the respective particle images, where a sine fit of the gray-value distributions also enables the quantification of fringe portions. The determined fringe numbers are provided above the respective fringe patterns of Figure 4, whereas the resulting bubble diameter estimations

according to Equation (2) are provided below the respective patterns. Note that the most right fringe patterns belongs to the converging part of the annular gap at the far right of the observed FOV, where the gap height is significantly larger than the nominally investigated $h = 400\,\mu m$ gap height. Since the optical system and corresponding astigmatic effect on the optical transfer functions also influences the diameter determination process, the provided numbers below the respective fringe patterns, as yet, only serve as an order of magnitude estimation of the bubble-sizing effort.

4. Concluding Remarks

The presented proof-of-concept study reveals various insights regarding future efforts in the field of laser-optical flow diagnostics in RPDCs. Most importantly, the two tested DPTV and IPI appear promising experimental approaches for the investigation of the given flow scenario - even though it becomes obvious from today's perspective that either measurement technique needs to be substantially revised, improved and/or adapted for the given test scenario of wide aspect-ratio rotor-stator shear flow across curved annular sub-millimeter gaps.

The scatter margin of the Hough-Transform diameter-estimation indicates the impact of the astigmatic influence of the curved stator wall resulting particle images. However, even the present level of processing accuracy saliently demonstrates the applicability of DPTV for the investigation of velocity fields across thin annular rotor-stator gaps. Future efforts foresee particular extension of the standard Hough-Transform to the particular detection of ellipses, where the combination of the semi-major and semi-minor axes will be considered simultaneously. In addition, these efforts will also take complementary advantage of the recently developed data-processing knowledge of the astigmatism particle tracking velocimetry (APTV) [18, 19], which interprets the particle-image shape rather than its diameter for depth codification.

The presented IPI tests demonstrated the general persistence of the fringe pattern across the curved transparent wall. However, similar to the calibration of any advanced particle-image detection effort, also the IPI post processing requires a careful and in-depth revision and reconsideration of all involved processing steps before a quantitative evaluation of the recorded fringes becomes possible. For instance, the inclined illumination beam refracts towards the radial coordinate into the stator wall (and the fluid). As such, the bubbles do not encounter parallel light, which in turn requires further elaboration of the underlying geometrical optics for advance data processing beyond the present level of standard treatment as outlined in Equation (4). This influential factor is foreseen to be further affected by the laser-beam diameter and correspondingly varying refraction angle over the beam cross-section upon inclined impact onto
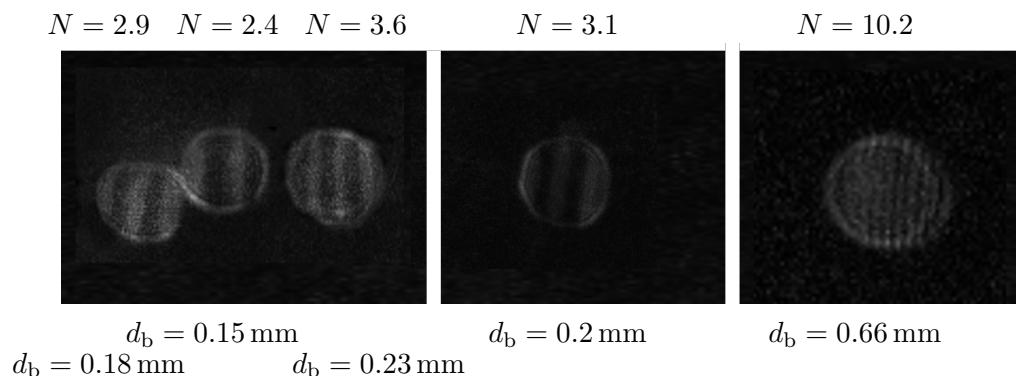

$N = 2.9$ $N = 2.4$ $N = 3.6$ $N = 3.1$ $N = 10.2$

$d_b = 0.15\,mm$ $d_b = 0.2\,mm$ $d_b = 0.66\,mm$

$d_b = 0.18\,mm$ $d_b = 0.23\,mm$

Figure 4. Raw data of IPI with corresponding fringe number N and approximated diameter d_b according to Equation (4).

a curve air-glass interface.

Once expanded towards a robust quantitative bubble-sizing approach for thin annular gaps, the IPI method seems also particularly candidating to provide void-fraction (-distribution) information, since location and diameter of the IPI-bubbles can be further converted into gas volumes in the known observed liquid volume. For statistically significant amounts of data such information is foreseen to lead to robust information of the void-fraction distribution.

As a final conclusion, despite the present premature quality of a feasibility study, the achieved results and uncovered insights of the investigation provide a clear outline of the IPI and DPTV to be an ideal combination to analyze complex wide aspect-ratio gap-flow scenarios. Future investigations will, therefore, address the outlined processing strategies so as to make the DPTV-IPI combination accurately applicable for both the presented annular gap flow (e.g. housing gap of RPDCs) but also for planar rotor-stator gaps (e.g. front gap of RPDCs).

References

[1] Xin D, Feng J, Jia X and Peng X 2010 An investigation into oil—gas two-phase leakage flow through micro gaps in oil-injected compressors *Proceedings of the Institution of Mechanical Engineers, Part C: Journal of Mechanical Engineering Science* **224** 925–933 URL https://doi.org/10.1243/09544062JMES1704

[2] Vasuthevan H and Brümmer A 2019 Generic experimental investigation of hydraulic losses within twin-screw machines *The 9th International Conference on Compressor and Refrigeration.* **Xi'an (China)** 10pp

[3] Leister R, Fuchs T, Mattern P and Kriegseis J 2021 Flow-structure identification in a radially grooved open wet clutch by means of defocusing particle tracking velocimetry *Experiments in Fluids* **62** 29 URL https://doi.org/10.1007/s00348-020-03116-0

[4] Fuchs T, Hain R and Kähler C J 2016 In situ calibrated defocusing ptv for wall-bounded measurement volumes *Measurement Science and Technology* **27** 084005 URL https://doi.org/10.1088/0957-0233/27/8/084005

[5] Fuchs T, Hain R and Kähler C J 2016 Uncertainty quantification of three-dimensional velocimetry techniques for small measurement depths *Experiments in Fluids* **57** 73 URL https://doi.org/10.1007/s00348-016-2161-5

[6] Tropea C 2011 Optical particle characterization in flows *Annual Review of Fluid Mechanics* **43** 399–426 URL https://doi.org/10.1146/annurev-fluid-122109-160721

[7] Fansler T D and Parrish S E 2014 Spray measurement technology: a review *Measurement Science and Technology* **26** 012002 URL https://doi.org/10.1088/0957-0233/26/1/012002

[8] Dehaeck S and van Beeck J 2008 Multifrequency interferometric particle imaging for gas bubble sizing *Experiments in Fluids* **45** 1432–1114 URL https://doi.org/10.1007/s00348-008-0502-8

[9] Kawaguchi T, Akasaka Y and Maeda M 2002 Size measurements of droplets and bubbles by advanced interferometric laser imaging technique *Measurement Science and Technology* **13** 308–316 URL https://doi.org/10.1088/0957-0233/13/3/312

[10] Raffel M, Willert C E, Scarano F, Kähler C J, Wereley S T and Kompenhans J 2018 *Particle Image Velocimetry* (Springer-Verlag GmbH) URL https://doi.org/10.1007/978-3-319-68852-7

[11] Willert C E and Gharib M 1992 Three-dimensional particle imaging with a single camera *Experiments in Fluids* **12** 353–358 URL https://doi.org/10.1007/BF00193880

[12] Olsen M G and Adrian R J 2000 Out-of-focus effects on particle image visibility and correlation in microscopic particle image velocimetry *Experiments in Fluids* **29** S166–S174 URL https://doi.org/10.1007/s003480070018

[13] Hough P V C 1959 Machine Analysis of Bubble Chamber Pictures *Proceedings, 2nd International Conference on High-Energy Accelerators and Instrumentation* **C590914** 554–558 URL https://s3.cern.ch/inspire-prod-files-5/53d80b0393096ba4afe34f5b65152090

[14] König G, Anders K and Frohn A 1986 A new light-scattering technique to measure the diameter of periodically generated moving droplets *Journal of Aerosol Science* **17** 157–167 URL https://www.sciencedirect.com/science/article/pii/0021850286900637

[15] Ragucci R, Cavaliere A and Massoli P 1990 Drop sizing by laser light scattring exploiting intensity angular oscillation in the mie regime *Particle & Particle Systems Characterization* **7** 221–225

[16] Leister R and Kriegseis J 2019 *Proceedings of the 13th International Symposium on Particle Image Velocimetry* ed Kähler C J, Hain R, Scharnowski S and Fuchs T URL https://athene-forschung.unibw.de/doc/129141/129141.pdf

[17] Spurk J H and Aksel N 2020 *Fluid Mechanics, 8: Hydrodynamic Lubrication* (Springer International Publishing) pp 251–283 URL https://doi.org/10.1007/978-3-030-30259-7_8

[18] Cierpka C, Rossi M, Segura R and Kähler C J 2011 On the calibration of astigmatism particle tracking velocimetry for microflows *Measurement Science and Technology* **22** 015401 URL http://stacks.iop.org/0957-0233/22/i=1/a=015401

[19] Rossi M and Kähler C J 2014 Optimization of astigmatic particle tracking velocimeters *Experiments in Fluids* **55** URL https://doi.org/10.1007/s00348-014-1809-2